engineering proceedings

Proceeding Paper

Centrifugal RPM as an Active Phase-Selection Parameter in Liquid-Phase-Exfoliated Graphene †

Maryam Basit [1], Sofia Javed [1,*] and Muhammad Aftab Akram [2]

[1] School of Chemical & Materials Engineering, National University of Science & Technology, Islamabad 44000, Pakistan; m.maryambasit@gmail.com
[2] Department of Materials Science & Engineering, Pak-Austria Fachhochschule, Institute of Applied Science & Technology, Haripur 22650, Pakistan; aftab.akram@fcm3.paf-iast.edu.pk
* Correspondence: sofia.javed@scme.nust.edu.pk
† Presented at the 7th Conference on Emerging Materials and Processes (CEMP 2026), Islamabad, Pakistan, 9–10 February 2026.

Abstract

Liquid-phase exfoliation is used as a scaled-up method for graphene synthesis; centrifugal separation is used as a thickness sorting process. RPM induces changes in interlayer coherence, defect density, morphology, and surface chemistry, as revealed by a systematic analysis of structure, morphology, and surface chemistry. This indicates selective attenuation of functionalization, leading to increased optical transparency. High RPMs increase the prevalence of basal-plane structures and yield enlarged graphene structures with lower edge disorder, whereas low RPMs maintain a stacked structure with a higher defect ratio. Therefore, RPM can be used as an adjustable kinetic parameter in the manufacture of graphene.

Keywords: liquid-phase exfoliation; 2D material; RPM-controlled centrifugation; phase selection; defect engineering

1. Introduction

Graphene has attracted significant interest due to its outstanding electrical, optical, and mechanical properties. However, exploiting graphene for real-world applications is limited by challenges in scalable production [1–3]. Liquid-phase exfoliation (LPE) of graphite is one of the most considered and cost-effective routes, and the most suitable in terms of industry suitability [1,4,5]. Nonetheless, LPE produces polydisperse graphene dispersions with wide distributions in thickness, lateral dimensions, defect density, and surface chemistry, and thus requires post-exfoliation separation processes to achieve homogeneous distributions of these properties [2,6,7].

Routine centrifugation is performed post-LEP but should be viewed as a mechanism for thickness-dependent size sorting [7–9]. This reduced description ignores the combined effects of hydrodynamic forces, interlayer adhesion, defect topology, and surface energetics, all of which define the stability of graphene in liquid systems [10,11]. As a result, the effect of rotational velocity on the structural and chemical properties of the separated graphene fractions remains poorly studied.

The evidence suggests that graphene performance is not determined solely by the number of layers [12]. The defect density, edge-to-basal-plane ratio, oxygen-based surface groups, and structural crystallinity play critical roles in the performance of graphene [5,13]. Notably, these qualities are subject to exfoliation processes and separation environment, and a thickness does not always correlate with order or crystallinity [14] This indicates that

Check for updates

Academic Editors: Muhammad Salman Haider, Muhammad Ahsan and Iftikhar Ahmad

Published: 16 November 2026

Copyright: © 2026 by the authors. Licensee MDPI, Basel, Switzerland. This article is an open access article distributed under the terms and conditions of the Creative Commons Attribution (CC BY) license.

centrifugation can selectively enrich populations of graphene with specific structural and chemical phases beyond simple layer-number control [5,12].

This study aims to redefine centrifugation as a phase-selective form of fractionation rather than a purely mechanical sorting process [15,16]. The forces on graphene flakes in a centrifugal field are controlled by size, mass, and interparticle interactions; therefore, they enable selective retention or sedimentation of sheets with specific defect distributions, interlayer forces, and surface functionalization [17]. Based on this, high RPMs could be used to isolate crystallographic coherent, basal-plane-dominated graphene, while low RPMs could be used to maintain populations rich in edges and defects [14,18]. Although theoretically plausible, these differences have rarely been confirmed by systematic experimental studies that use complementary structural, spectroscopic, and optical studies.

In the current work, we show that centrifugal separation, which is a process controlled by RPM in the LPE process, is an active process of phase-selection, which selects structural and chemical phases of graphene and thus overcomes the traditional, thickness-based sorting regime [15,19]. Through systematic change and isolation of rotational speed, we find a nonlinear dependence between crystallinity, defect density, surface functionalization, and optical properties. The change in interlayer distance and crystalline coherence due to rotational velocity is measured through X-Ray Diffraction (XRD) [10,20], and the change in edges and defects is measured on a Raman spectrum [5]. Scanning Electron Microscopy (SEM) is used to determine morphological differences between the fractionated samples [8], and Fourier-Transform Infrared (FTIR) spectroscopy combined with X-Ray Photoelectron Spectroscopy (XPS) provides information on surface chemistry [10,20], which depends on RPM.

We have refuted the ancient paradigm of LPE graphene processing, where the main emphasis has been on thickness, and established centrifugal RPM as a parameter to be regulated to obtain active phase selection [1,15]. The product results in a scalable, non-chemisorption-based method to manipulate the properties of graphene to enable full-scale control of the population of defect-rich and defect-free particles to match application needs [5,10]. In a wider sense, the conceptualization of centrifugal separation in this article is more of a material design concept and not a post-synthesis procedure, thus facilitating the mass production of functional two-dimensional carbon materials.

2. Synthesis of Graphene

Graphene fabrication was done using an improved top-down LPE process. In total, 80 g of 1-methyl-2-pyrrolidone (NMP) was combined with 1 g of high-purity graphite powder (particle size < 150 μm, purity 99.99%) under ambient laboratory conditions. The suspension was then sonicated for 12 h, allowing for the delamination of the graphite layers into few-layer sheets of graphene. After sonication, the suspension was centrifuged at 1000, 2000, 3000, and 4000 RPM, allowing the different sub-populations of graphene with different structural properties to be separated. The supernatant was carefully washed with acetone and ethanol to remove the residual solvent and loosely attached impurities. Lastly, the samples were dried at 60 °C to reduce thermal perturbations of the graphene architecture.

3. Results and Discussion

3.1. Scanning Electron Microscopy (SEM)

SEM reveals a distinct RPM-dependent morphological change in graphene during LPE. Thick, compact, and strongly restacked multilayer platelets prevail at 1000 RPM in Figure 1a, which indicates a lack of shear power to reduce interlayer van der Waals interactions [7,20]. In Figure 1b, these are partially delaminated at 2000 RPM, with stepped edges, surface roughening, and coexisting thick–thin domains formed due to selective sedimentation

caused by mass and hydrodynamic drag [3,10]. The highest-RPM fractions are thin and wrinkled, loosely stacked sheets of graphene with reduced lateral size and an elevated edge density, as in few-layer graphene Figure 1c,d. Significantly, physical exfoliation is confirmed by the absence of amorphization without lattice collapse [4,5,15], which defines RPM as an active phase-selection parameter governing thickness, stacking, and surface exposure.

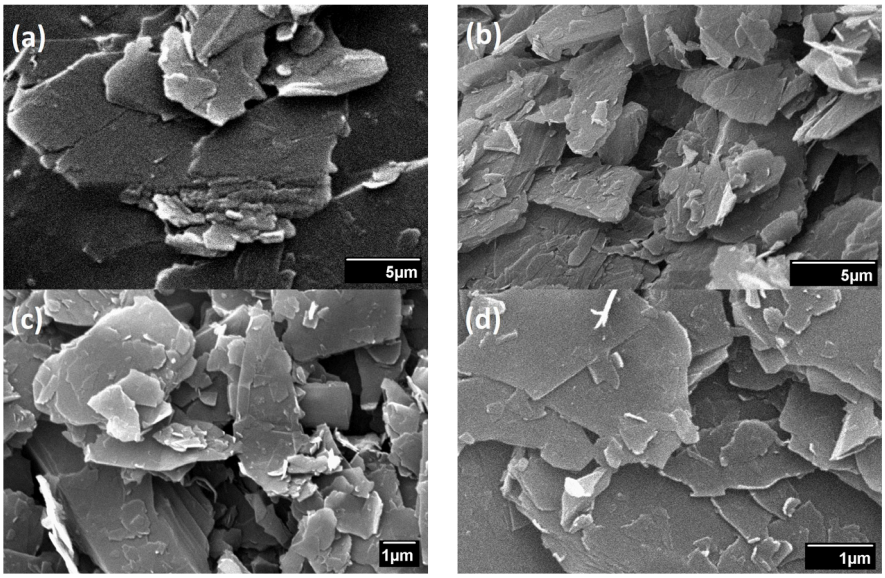


Figure 1. SEM micrographs of graphene fractions are isolated at different centrifugal speeds: (**a**) 1000 RPM, (**b**) 2000 RPM, (**c**) 3000 RPM and (**d**) 4000 RPM-driven on morphological bases.

3.2. X-Ray Photoelectron Spectroscopy (XPS)

XPS was used to investigate the influence of centrifugal speed on the surface chemistry of graphene fractions obtained by LPE. The preponderance of carbon and only minor oxygen contributions in all samples, confirmed by survey spectra, eliminates bulk chemical oxidation during exfoliation. C1s spectra were deconvoluted into sp^2 C=C (284.4–284.6 eV), sp^3 C-C/C-H, C-O, and C=O/COO functionality (close to 287.8, 288.3 eV). At low RPM in Figure 2a, fractions exhibit a strong sp^2 peak with suppressed oxygenated signals, along with thick, restacked graphitic domains and strong (00l) stacking in the XRD data. The limited contributions of C and C=O increase with increasing RPM in Figure 2b–d, with the sp^2 framework remaining strong due to greater edge exposure and the accessibility of more surfaces on thinner sheets, as opposed to disruptive oxidation [1,21]. The lack of strong epoxy and carboxyl groups indicates that surface functionalization is restricted. Overall, XPS shows that centrifugal RPM acts as a physical filter for thickness and surface accessibility and thus confirms phase-separation control in LPE by RPM.

3.3. Fourier Transformation Infrared (FTIR)

To support the explanation of the centrifugal-speed-dependent dynamics of the surface functional group on LPE graphene, FTIR is complemented by XPS results. In Figure 3a the low-RPM fractions have a broad OH stretching band in the 3200–3600 cm^{-1} range, suggesting the presence of the hydroxyl groups and physiosorbed moisture, which is confirmed by the increase in the C1s and the C-OH features at 286.2 eV in the XPS spectra, displaying the oxygen enrichment on the exposed basal planes and interlayers [20]. Absorption bands at about ~2920 and ~2850 cm^{-1} C–C/C–H vibrational bands respectively, which are deemed to represent the presence of residual solvent and adventitious carbon, respectively, and diminish with increasing rotational frequency, confirming effective non-graphitic removable residue

removal [21]. The carbonyl stretching band found in the 1720–1740 cm^{-1} attributed to the C=O stretch of the carboxyl and carbonyl group range is strong in low-RPM fractions and fades away with acceleration, which indicates that oxidative functionalization decreases with greater thinness in fraction dispersion [20]. Another strong sp^2 C=C vibrational mode between 1620 and 1580 cm^{-1} further confirms the retention of a conjugated carbon framework [21], findings which correspond to the strong X-Ray Diffraction (002) reflexes and the prevalent sp^2 signatures in the XPS spectra. Taken together, the FTIR spectra indicate a rotational-period-dependent shift of oxygen-rich graphitic stacks toward cleaner, electronically intact graphene sheets. Table 1 gives an overview of the FTIR spectra analysis at different RMP speeds.

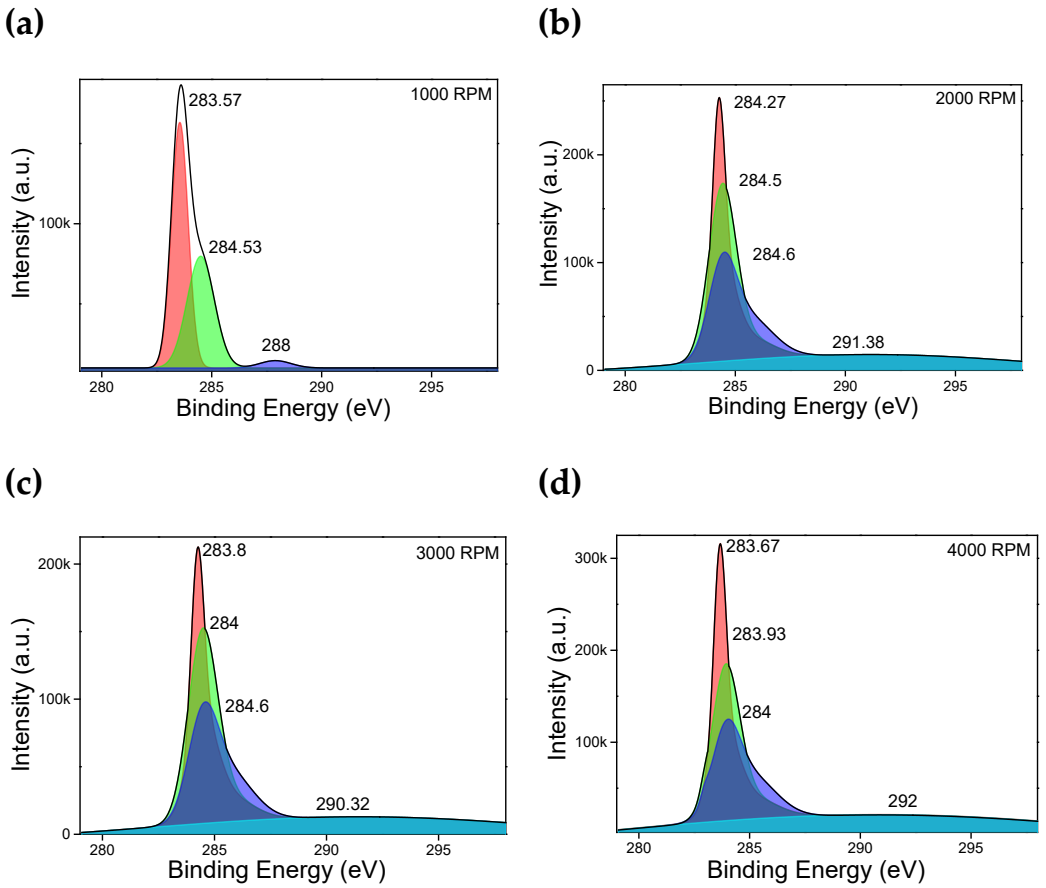


Figure 2. XPS spectra of RPM-separated graphene fractions showing centrifugal-speed-dependent surface phase selection: (**a**) 1000 RPM, (**b**) 2000 RPM, (**c**) 3000 RPM and (**d**) 4000 RPM.

Table 1. FTIR assignment of the effects of centrifugal speed on graphene separated at different RPM speeds.

FTIR Band (cm^{-1})	Bonding	Corresponding Peaks	Binding Energy (eV)	Interpretation
3200–3600	O–H stretching	C–OH	~286.1–286.5	Hydroxylated surface carbons, adsorbed oxygen species
2920–2850	C–H stretching	C–C/C–H	~284.6–284.8	Residual sp^2/sp^3 carbon and solvent-derived moieties
1720–1740	C=O stretching	C=O/O–C=O	~287.8–289.0	Carbonyl and carboxyl groups from oxidative damage
1620–1580	C=C stretching	sp^2 C=C	~284.4–284.6	Graphitic backbone, long-range order
1220–1050	C–O–C/C–O	C–O	~286.5–287.2	Epoxy and alkoxy defect sites

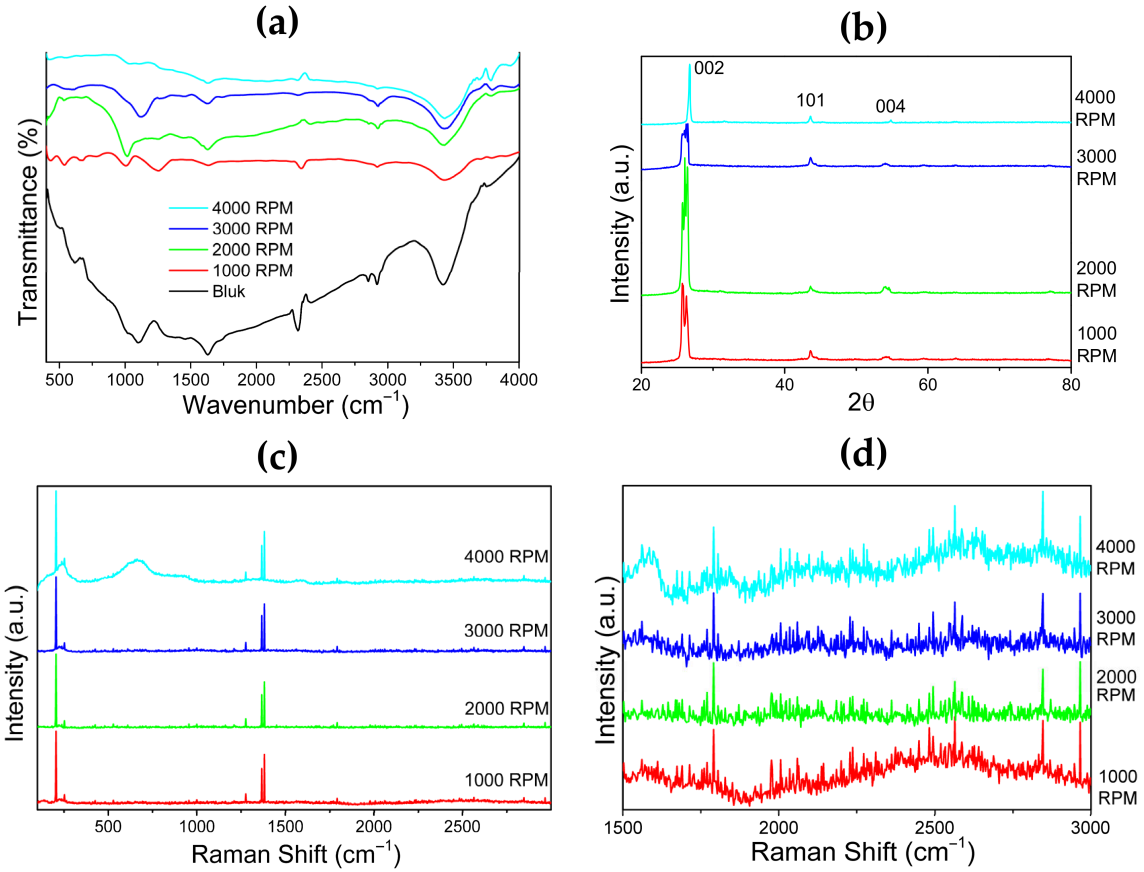


Figure 3. (**a**) FTIR spectra, (**b**) XRD patterns, (**c**) full Raman and (**d**) Raman from 1500 to 3000 cm^{-1} of RPM-separated graphene fractions revealing centrifugal-speed-driven surface phase evolution.

3.4. X-Ray Diffraction (XRD)

XRD was used to characterize phase and stacking changes in the fractions of graphene obtained by centrifugation at different RPMs following LPE. The retention of the hexagonal graphite structure and the absence of oxide- or catalyst-derived phases were confirmed by the fact that all measured samples had a discrete (002) reflection [19]. Regular changes in the maximum amplitude, width, and location indicate that the centrifugal RPM is an active modulator of interlayer coupling rather than a passive thickness-based sorting mechanism. In Figure 3b the fractions with low RPM had a sharp (002) peak, indicating that the material has high interlayer coherence, large crystallite domains, and weakly exfoliated graphite restacking. The (002) reflection became successively broader and weaker, which is also expected of a shorter coherence length and partial interlayer relaxation by efficient delamination. Significantly, there was no evidence of amorphous carbon and peak collapse, indicating that centrifugation does not affect the integrity of the lattices. The (002) remains persistent, with a remarkable increase in intensity at 2000 RPM. This indicates a redistribution of stacking order rather than progressive crystallinity degradation with RPM increase. In summary, XRD confirms that centrifugal RPM is a dynamic selector of graphitic phase identity and interlayer organization [19].

3.5. Raman Spectroscopy

Raman spectroscopy was to be used, and the structural variations in the LPE graphene fractions isolated at different centrifugal speeds were to be analyzed. The features of graphitic carbon D (~1350 cm^{-1}), G (~1580 cm^{-1}), and 2D (~2700 cm^{-1}) bands [21] are observed in all samples, but systematic changes in intensity, linewidth, and background pro-

files demarcate the phases selected by RPM in Figure 3c,d. A strong G band, an attenuated D band, and a weak, broadened 2D feature can be observed in low-RPM fractions, which represent multilayer, strongly stacked graphene. Rising RPM is accompanied by shifts in the D-band and G-band intensities, as reflected in the I_{2D}/I_G ratio, indicating that the densification of edges and thinning of the thickness are caused by shear-induced fragmentation, whereas basal-plane disorder does not vary. The G-band location in the image is symmetric and stable, indicating that the sp^2 lattice is maintained [21]. Successful delamination and poor interlayer bonding are indicated by the intensification of the 2D band at high RPM. These peaks define the centrifugal speed as an activated-phase-selection parameter. This varies defect topology, stacking interactions, and graphene thickness without affecting inherent structural integrity. Table 2 shows the overall view of the Raman spectra analysis at different RMP speeds.

Table 2. Raman spectral parameters of graphene fractions isolated at different centrifugal RPM.

Sample	D Band (cm^{-1})	G Band (cm^{-1})	2D Band (cm^{-1})	I_D/I_G	I_{2D}/I_G	Structural Interpretation
4000 RPM	1366	~1791	~2845	9.7	1.95	Edge-dominated, highly exfoliated; turbostratic stacking
3000 RPM	1366	~1791	~2844	8.5	1	Thickness-reduced graphene; increased edge contribution
2000 RPM	1356	~1791	~2846	10	0.86	Few-layer graphene; partial delamination; coherent stacking
1000 RPM	1354	~1791	~2845	7.2	0.6	Bulk-like graphitic domains; strong stacking; low edge density

4. Conclusions

This study establishes centrifugal RPM as an intrinsic and tunable phase-selection parameter in liquid-phase exfoliated graphene rather than a passive separation step. Raman analysis across all fractions confirms preservation of the sp^2 graphitic framework while revealing systematic, RPM-dependent modulation of defect density, interlayer coupling, and layer thickness. The progressive evolution from stacked, multilayer graphene at low RPM to electronically decoupled few-layer graphene at high RPM arises from controlled shear-induced delamination and edge activation, not from basal-plane disorder or structural degradation. The consistency of Raman signatures across both spectra reinforces the reproducibility and robustness of this mechanism. These findings provide a mechanistically grounded strategy for phase-resolved graphene production, enabling precise tailoring of structural quality through centrifugal control alone and offering a scalable route for application-specific graphene engineering.

Author Contributions: M.B., methodology, formal analysis, investigation, data curation, writing—original draft preparation, and visualization, S.J.; resources, supervision, project administration, writing—review and editing, and M.A.A., validation. All authors have read and agreed to the published version of the manuscript.

Funding: This research received no external funding.

Institutional Review Board Statement: Not applicable.

Informed Consent Statement: Not applicable.

Data Availability Statement: Dataset available on request from the authors.

Acknowledgments: During the preparation of this manuscript, the author(s) used Grammarly pro for language editing and grammar refinement. The authors have reviewed and edited the output and take full responsibility for the content of this publication.

Conflicts of Interest: The authors declare no conflicts of interest.

References

1. Li, Z.; Young, R.J.; Backes, C.; Zhao, W.; Zhang, X.; Zhukov, A.A.; Tillotson, E.; Conlan, A.P.; Ding, F.; Haigh, S.J.; et al. Mechanisms of Liquid-phase exfoliation for the Production of Graphene. *ACS Nano* **2020**, *14*, 10976–10985. [CrossRef] [PubMed]
2. Hu, C.-X.; Shin, Y.; Read, O.; Casiraghi, C. Dispersant-assisted liquid-phase exfoliation of 2D materials beyond graphene. *Nanoscale* **2021**, *13*, 460–484. [CrossRef] [PubMed]
3. Nastran, M.; Peschek, P.; Walendzik, I.; Rath, J.; Fickl, B.; Schubert, J.S.; Ipsmiller, W.; Bartl, A.; Mauschitz, G.; Szabo, G.; et al. Liquid phase exfoliation of graphene using ammonia as an easy-to-remove additive in low-boiling organic-water co-solvent suspensions. *Commun. Chem.* **2025**, *8*, 161. [CrossRef] [PubMed]
4. Xu, Y.; Cao, H.; Xue, Y.; Li, B.; Cai, W. Liquid-phase exfoliation of graphene: An overview on exfoliation media, techniques, and challenges. *Nanomaterials* **2018**, *8*, 942. [CrossRef] [PubMed]
5. Ng, K.L.; Maciejewska, B.M.; Qin, L.; Johnston, C.; Barrio, J.; Titirici, M.-M.; Tzanakis, I.; Eskin, D.G.; Porfyrakis, K.; Mi, J.; et al. Direct Evidence of the Exfoliation Efficiency and Graphene Dispersibility of Green Solvents toward Sustainable Graphene Production. *ACS Sustain. Chem. Eng.* **2023**, *11*, 58–66. [CrossRef] [PubMed]
6. Fang, X.; Pang, K.; Zhao, G.; Wang, Y.; Zhang, W.; Zhang, Y.; Zhou, S.; Zhang, J.; Gong, C. Improving the liquid phase exfoliation efficiency of graphene based on the enhanced intermolecular and interfacial interactions. *Chem. Eng. J.* **2024**, *480*, 148263. [CrossRef]
7. Arifutzzaman, A.; Ismail, A.F.; Alam, M.Z.; Khan, A.A.; Rahman, S. Investigation of Extraction Yields of Exfoliated Graphene in Deionized Water from Organic Solvents. *Int. J. Technol.* **2019**, *10*, 1251–1259. [CrossRef]
8. Khan, U.; O'neill, A.; Porwal, H.; May, P.; Nawaz, K.; Coleman, J.N. Size selection of dispersed, exfoliated graphene flakes by controlled centrifugation. *Carbon* **2012**, *50*, 470–475. [CrossRef]
9. Oshima, K.; Nakamura, K.; Guo, H.; Smith, R.L. Mini-review on application of analytical centrifugation, ultracentrifugation and centrifugal devices to phase equilibria and separation processes. *Fluid Phase Equilibria* **2022**, *558*, 113457. [CrossRef]
10. Saeed, M.A.; Ismai, A.A.; Alsaidi, M.; Ahmad, S. Liquid-phase exfoliation of graphite using various surfactants into few-layer graphene. *Mater. Chem. Phys.* **2025**, *348*, 131650. [CrossRef]
11. Verma, A.K.; Sharma, B.B. Experimental and Theoretical Insights into Interfacial Properties of 2D Materials for Selective Water Transport Membranes: A Critical Review. *Langmuir* **2024**, *40*, 7812–7834. [CrossRef] [PubMed]
12. Sahoo, P.; Matte, H.S.S.R. Solution-based exfoliation of non-layered, non-van der Waals materials and applications: Current status and future directions. *J. Mater. Chem. C* **2025**, *13*, 22515–22538. [CrossRef]
13. Deerattrakul, V.; Hirunpinyopas, W.; Pisitpipathsin, N.; Saisopa, T.; Sawangphruk, M.; Nualchimplee, C.; Iamprasertkun, P. The electrochemistry of size dependent graphene *via* liquid phase exfoliation: Capacitance and ionic transport. *Phys. Chem. Chem. Phys.* **2021**, *23*, 11616–11623. [CrossRef] [PubMed]
14. Hu, C.-X.; Read, O.; Shin, Y.; Chen, Y.; Wang, J.; Boyes, M.; Zeng, N.; Panigrahi, A.; Kostarelos, K.; Larrosa, I.; et al. Effects of Lateral Size, Thickness, and Stabilizer Concentration on the Cytotoxicity of Defect-Free Graphene Nanosheets: Implications for Biological Applications. *ACS Appl. Nano Mater.* **2022**, *5*, 12626–12636. [CrossRef] [PubMed]
15. Goldie, S.; Ott, S.; Dawson, A.; Starke, T.; Gabbett, C.; Vega-Mayoral, V.; Synnatschke, K.; Horn, M.; Coleman, J.N.; Backes, C. Centrifugation Theory Revisited: Understanding and Modeling the Centrifugation of 2D Nanosheets. *Adv. Mater. Interfaces* **2025**, *12*, e00717. [CrossRef]
16. Caffrey, E.; Munuera, J.M.; Gabbett, C.; Doolan, L.; Neilson, J.; Wells, R.A.; McCrystall, M.; McNamara, A.; Carey, T.; Gerlei, M.; et al. Quantifying the Influence of Nanosheet Aspect Ratio on Network Morphology and Junction Resistance in Solution-Processed Nanosheet Networks. *ACS Nano* **2025**, *19*, 33118–33133. [CrossRef] [PubMed]
17. Perez-Alvarez, D.T.; Marchesini, S.; Paton, K.R.; Sykes, J.; Hampel, D.; Burt, J.; Despotelis, K.; Fernandes, D.; Davies, P.; Windows-Yule, C.; et al. Predicting graphene production with population balance modelling. *Carbon* **2025**, *231*, 119687. [CrossRef]
18. Krasnova, A.O.; Glebova, N.V.; Nechitailov, A.A.; Kastsova, A.G.; Pelageikina, A.O.; Kirilenko, D.A.; Shvidchenko, A.V.; Shestakov, M.S.; Koroleva, A.V.; Khrapova, E.K. Comparative Study of Graphite Exfoliation Techniques Using Nafion as a Surfactant. *C* **2025**, *11*, 76. [CrossRef]
19. Güler, Ö.; Tekeli, M.; Taşkın, M.; Güler, S.H.; Yahia, I. The production of graphene by direct liquid phase exfoliation of graphite at moderate sonication power by using low boiling liquid media: The effect of liquid media on yield and optimization. *Ceram. Int.* **2021**, *47*, 521–533. [CrossRef]

20. Rico, J.; Castaño-Soto, M.; Lopez-Arango, N.; Hernandez, Y. Influence of C=O groups on the optical extinction coefficient of graphene exfoliated in liquid phase. *J. Phys. Condens. Matter* **2022**, *34*, 105701. [CrossRef] [PubMed]
21. Sethurajaperumal, A.; Varrla, E. High-Quality and Efficient Liquid-Phase Exfoliation of Few-Layered Graphene by Natural Surfactant. *ACS Sustain. Chem. Eng.* **2022**, *10*, 14746–14760. [CrossRef]

Disclaimer/Publisher's Note: The statements, opinions and data contained in all publications are solely those of the individual author(s) and contributor(s) and not of MDPI and/or the editor(s). MDPI and/or the editor(s) disclaim responsibility for any injury to people or property resulting from any ideas, methods, instructions or products referred to in the content.